Journal of Hydrology 523 (2015) 196–210

Contents lists available at ScienceDirect

Journal of Hydrology

journal homepage: www.elsevier.com/locate/jhydrol

Catchment response to bark beetle outbreak and dust-on-snow in the Colorado Rocky Mountains

Ben Livneh [a,b,*], Jeffrey S. Deems [a,b,c], Brian Buma [d], Joseph J. Barsugli [a,b,e], Dominik Schneider [f], Noah P. Molotch [f,g], K. Wolter [e], Carol A. Wessman [a,b]

[a] Cooperative Institute for Research in Environmental Science (CIRES), University of Colorado, Boulder, 216 UCB, Boulder, CO 80309, United States
[b] Western Water Assessment (WWA), University of Colorado, Boulder, 216 UCB, Boulder, CO 80309, United States
[c] National Snow and Ice Data Center (NSIDC), University of Colorado, Boulder, 449 UCB, Boulder, CO 80309-0449, United States
[d] Dept. of Natural Sciences, University of Alaska Southeast, 11120 Glacier Hwy, Juneau, AK 99801, United States
[e] NOAA Earth System Research Laboratory, Physical Sciences Division, 325 Broadway, Boulder, CO 80309, United States
[f] Department of Geography, Institute of Arctic and Alpine Research (INSTAAR), University of Colorado, Boulder, 450 UCB, Boulder, CO 80309-0450, United States
[g] Jet Propulsion Laboratory, California Institute of Technology, 4800 Oak Grove Dr., Pasadena, CA 91109, United States

ARTICLE INFO

Article history:
Received 24 July 2014
Received in revised form 7 January 2015
Accepted 17 January 2015
Available online 2 February 2015
This manuscript was handled by Konstantine P. Georgakakos, Editor-in-Chief, with the assistance of Yasuto Tachikawa, Associate Editor

Keywords:
Forest disturbance
Catchment hydrology
Bark beetle
Dust on snow
Hydrologic modeling

SUMMARY

Since 2002, the headwaters of the Colorado River and nearby basins have experienced extensive changes in land cover at sub-annual timescales. Widespread tree mortality from bark beetle infestation has taken place across a range of forest types, elevation, and latitude. Extent and severity of forest structure alteration have been observed through a combination of aerial survey, satellite remote-sensing, and in situ measurements. Additional perturbations have resulted from deposition of dust from regional dry-land sources on mountain snowpacks that strongly alter the snow surface albedo, driving earlier and faster snowmelt runoff. One challenge facing past studies of these forms of disturbance is the relatively small magnitude of the disturbance signals within the larger climatic signal. The combined impacts of forest disturbance and dust-on-snow are explored within a hydrologic modeling framework. We drive the Distributed Hydrology Soil and Vegetation Model (DHSVM) with observed meteorological data, time-varying maps of leaf area index and forest properties to emulate bark beetle impacts, and parameterizations of snow albedo based on observations of dust forcing. Results from beetle-killed canopy alteration suggest slightly greater snow accumulation as a result of less interception and reduced canopy sublimation and evapotranspiration, contributing to overall increases in annual water yield between 8% and 13%. However, understory regeneration roughly halves the changes in water yield. A purely observation-based estimate of runoff coefficient change with cumulative forest mortality shows comparable sensitivities to simulated results; however, positive water yield changes are not statistically significant ($p \leqslant 0.05$). The primary hydrologic impact of dust-on-snow forcing is an increased rate of snowmelt associated with more extreme dust deposition, producing earlier peak streamflow rates on the order of 1–3 weeks. Simulations of combined bark beetle and dust-on-snow produced little compounding effects, due to the relatively exclusive nature of their impacts. Potential changes in water yield and peak streamflow timing have important implications for regional water management decisions.

1. Introduction

The Colorado River Basin is an essential freshwater resource for the southern Rocky Mountains and U.S. Southwest, providing water supply to seven states and over 40 million people, and irrigation to roughly 5.5 million acres of farmland (Deems et al., 2013). The majority of water originates in the headwaters region and hence hydrologic changes to this region will impact downstream water availability. In the past decade, bark beetle species such as the mountain pine beetle (*Dendroctonus ponderosae*), spruce (*Dendroctonus rufipennis*) and *Ips* beetles have grown from endemic to epidemic levels, killing large areas of montane and subalpine forests. Across western North America, Bark Beetle (BB) related tree mortalities have affected an estimated 600,000 km^2 of forested watershed since 1996 (Bentz et al., 2009). Following a

* Corresponding author at: Cooperative Institute for Research in Environmental Science (CIRES), University of Colorado, Boulder, 216 UCB, Boulder, CO 80309, United States. Tel.: +1 303 497 5770.
E-mail address: ben.livneh@colorado.edu (B. Livneh).

http://dx.doi.org/10.1016/j.jhydrol.2015.01.039
0022-1694/

severely dry year in 2002 (Pielke et al., 2005), bark beetles have impacted more than 16,000 km^2 in Colorado (Pugh and Small, 2012), or roughly 2/5 of the forested watersheds. Broad interest has been lavished on the relationship of BB within forest ecosystems owing to their visible impacts on a range of sectors, including recreation, timber, fire risk, as well as water supply. Despite increasing BB research in recent years, comparatively few studies have examined the distributed impact of BB on hydrology over large areas. Meanwhile, recent episodic dust-on-snow events have been shown to alter snowmelt dynamics over a large portion of the basin headwaters for which hydrology is snowmelt-dominated (Deems et al., 2013; Painter et al., 2007, 2010, 2012a; Skiles et al., 2012). This combination of landscape-level disturbances raises the question of the relative magnitude of their effects and possible interactions. The work presented here explores a range of BB impacts together with dust-on-snow disturbances in several catchments within the Colorado River Basin headwaters and Colorado Front Range. Findings of local-impact studies using satellite and aerial-survey data are spatially integrated within a hydrologic modeling framework.

1.1. Bark beetles (BB)

Irrespective of geographical variations, the impact of BB infestations on a forest consists of five general stages. Here we describe the stages of the mountain pine beetle, which impacted three of the four study catchments, whereas the fourth catchment had minimal overall insect-related mortality. The first stage involves the initial attack of the beetles, in which females bore through the bark to the phloem and cambium region where the egg gallery is constructed (Alfaro et al., 2004). A beetle-borne fungus, the primary agent of mortality, produces a blue stain in the sapwood drastically disrupting water and sap flow in as short as ten days post-infestation (Hubbard et al., 2013). The second stage of impact, termed red-phase, begins with the onset of tree death (i.e. loss of transpiration) and lasts approximately one to three years as needles change in color from green to yellow to red, usually beginning in the tree crown (Wulder et al., 2006). Through the course of the red-phase, needles drop from the trees and reduce effective albedos of the cold-season snowpacks (Pugh and Gordon, 2012). Hydrologically important changes due to red-phase trees include: reduction in snow albedo due to needle litter, cessation of root water uptake and transpiration, reduction in canopy coverage and effective leaf area for moisture interception and radiative diffusion.

The end of red-phase is marked by complete needle loss, which marks the start of gray-phase, where trees appear as "skeletons" with only trunks and branches (Pugh and Gordon, 2012). The hydrologic alterations associated with the gray-phase include: recovery of sub-canopy snow albedo relative to red-phase due to cessation of needle litter (Boon, 2007; Pugh and Small, 2012), substantial loss of overstory canopy area leading to reduced canopy interception, decreased canopy snow sublimation, increased sub-canopy wind speeds, and greater radiation transmission through a diminished canopy (Pugh and Gordon, 2012). The gray-phase can last between roughly 4 and 20 years (Lewis and Hartley, 2006) before significant decay occurs. Enhanced regeneration of the understory has been observed progressively through the gray-phase, driven by water availability and sunlight exposure for the existing and new saplings (Collins et al., 2011).

Under unmanaged conditions, the gray phase may conclude following several different scenarios, such as increased risk for blow-down due to high winds and increased likelihood of fire due to higher fuel availability, although the latter has been disputed. Simard et al. (2011) showed that for lodgepole pine just north of the Colorado River Basin boundary (i.e. in Yellowstone National Park, USA), that BB outbreaks may *reduce* the probability of active crown fire in the short term by disconnecting adjacent tree crowns. The fourth and fifth stages are therefore concerned with degradation of dead biomass and complete regeneration of new forest, respectively. Given the broad range of uncertainties in these processes and their time horizons, the focus of this study is restricted to the impacts of the red and gray phases of BB infestation.

While there has been an abundance of stand-level work in beetle-kill forests, very few studies have attempted to spatially integrate BB impacts over larger scales (i.e. an entire catchment). Availability of satellite and remote sensing products over multi-year periods has enabled broader scale evaluations. For example, O'Halloran et al. (in press) used the Moderate Resolution Imaging Spectroradiometer (MODIS) imagery together with in situ observations to estimate changes in radiative forcings caused by BB tree mortality. Hicke and Jenkins (2008) used USDA Forest Service satellite classification to assess forest stand susceptibility to BB mortality. Other studies have used aerial (Ciesla, 2006; Meddens et al., 2011) or satellite imagery (White et al., 2005; Hicke and Logan, 2009; Dennison et al., 2010; Buma et al., 2013) to classify temporal patterns of BB into either total severity or into red and gray phases.

Another means to evaluate spatial impacts of BB on hydrology has been through modeling studies. Hydrologic modeling offers an attractive approach to assessing impacts, since it overcomes incongruences of paired-watershed studies (e.g. Bethlahmy, 1974; Stednick and Jensen, 2007), in effect making each watershed its own control, and also enables the integration of multiple streams of data, including meteorological, land cover, and geomorphic data. Recently, studies such as Alila et al. (2009) and Bewley et al. (2010) in British Columbia, Rudolph (2012) in Wyoming, Mikkelson et al. (2013), and Perrot et al. (2014) in Colorado, have simulated areal extents and severity of BB impacts.

1.2. Dust-on-snow

Rocky Mountain regional hydrology is dominated by the accumulation and melt of seasonal snowpacks. The energy exchange between the snowpack and the atmosphere, which governs the rate of snowmelt, is predominantly dictated by solar irradiance (Cline, 1997). Recent investigations have quantified snowmelt timing and runoff impacts due to perturbation of the mountain snowpack surface energy balance by deposition of mineral dust from regional dryland sources (Deems et al., 2013; Painter et al., 2007, 2010, 2012a, 2012b; Skiles et al., 2012). Dust loading strongly reduces the snow surface albedo, thus increasing absorption of incident solar radiation and influencing snowmelt runoff magnitude and timing. The aforementioned studies estimated hydrologic impacts of dust loading via point models and a relatively coarse-resolution distributed model (i.e. 12 km grid cells) informed by in situ measurements. All of the studies detail earlier peak streamflow associated with increasing dust loading. The full basin-scale modeling studies suggest decreasing annual water yield with increasing dust due to increased evaporative losses. Deems et al. (2013) suggest that dust-on-snow impacts may be further exacerbated by projected climate change. Unlike BB impacts, which are restricted to specific forest stands, dust-on-snow impacts are more spatially widespread.

It is hypothesized that BB-infestations may enhance the hydrologic impacts of dust-on-snow, since BB-related canopy reductions could increase the radiative exposure of sub-canopy snowpack and subsequently amplify the effect of dust-on-snow-driven snow albedo changes. Therefore, the objective of this work is to examine catchment-scale hydrologic response due to BB-induced alterations to forest structure, specifically during the red and gray phases, and to dust-on-snow influence on snow albedo. We

consider several forest disturbance scenarios that include remote-sensing-estimated outbreak patterns, as well as a hypothetical maximum understory regeneration scenario. We further combine the hydrologic impacts from the BB scenarios with several snow albedo scenarios representing various dust-on-snow loads in order to quantify their relative contributions to snowmelt perturbations separately and in combination. Catchment-scale (i.e. <500 km^2) sensitivities are presented using the Distributed Hydrology Soil and Vegetation Model (DHSVM; Wigmosta et al., 1994). Finally, an exclusively observation-based analysis is conducted (BB only) upon which modeling results are contrasted.

2. Methods

We used aerial survey, satellite, and in situ data to inform the DHSVM model of static and dynamic land cover states, dust-on-snow loading scenarios, and meteorological forcings. Model outputs were calibrated against streamflow observations once per basin before assessment of disturbance sensitivities, so that sensitivities could be expressed within the range of observed response. The simulations that are compared and discussed include: (i) vegetation disturbance scenarios of BB-driven canopy impacts—with and without understory regeneration—versus an undisturbed (full-canopy) case, and (ii) dust-on-snow scenarios for three loading severities—the same loading prescribed across all years—versus the most realistic, time-varying case, that uses a different dust scenario for each year.

2.1. Catchment description

Four study catchments were chosen on the basis of minimal anthropogenic disturbance, i.e. reservoir diversion and irrigation. Further, these catchments provide a range of climatologies, vegetation coverage, BB impacts, and dust-on-snow severities. Fig. 1 depicts the relative location of each catchment within the upper Colorado River Basin and Table 1 lists important characteristics. All catchments have snowmelt-dominated hydrology, characterized by a broad period of peak streamflow each year associated with snowmelt runoff. The fraction of each catchment impacted by beetle kill varied among catchments (Fig. 2) such that differing cumulative hydrologic sensitivities were anticipated. Descriptions of tree mortality observations together with parameterization of mortality into DHSVM are provided in Section 2.3.

2.2. DHSVM description and modeling approach

DHSVM was developed to simulate hydrologic processes in mountain catchments with relatively steep slopes, and has been applied over catchments on the order of 100–10,000 km^2, although typical implementations are for watersheds with areas less than 1000 km^2 (Carrasco and Hamlet, 2010). The model consists of a two-layer canopy representation for evapotranspiration (ET) and energy transfer, a two-layer energy balance model for snow accumulation and melt, a multilayer unsaturated soil model and a saturated subsurface flow model. DHSVM explicitly accounts for slope and aspect in characterizing shortwave and longwave radiation within the surface energy budget. The range of DHSVM inputs can be subdivided into three general categories: (i) land surface maps of vegetation, soil texture, geology, and topography (including monthly solar shading maps) and (ii) specification of coefficients and parameters for the various classes of land surface features and related processes; and (iii) timeseries of meteorological data (described in Section 2.6).

Notable developments of the DHSVM vegetation scheme were made by Storck et al. (1995, 1998), Wigmosta and Perkins

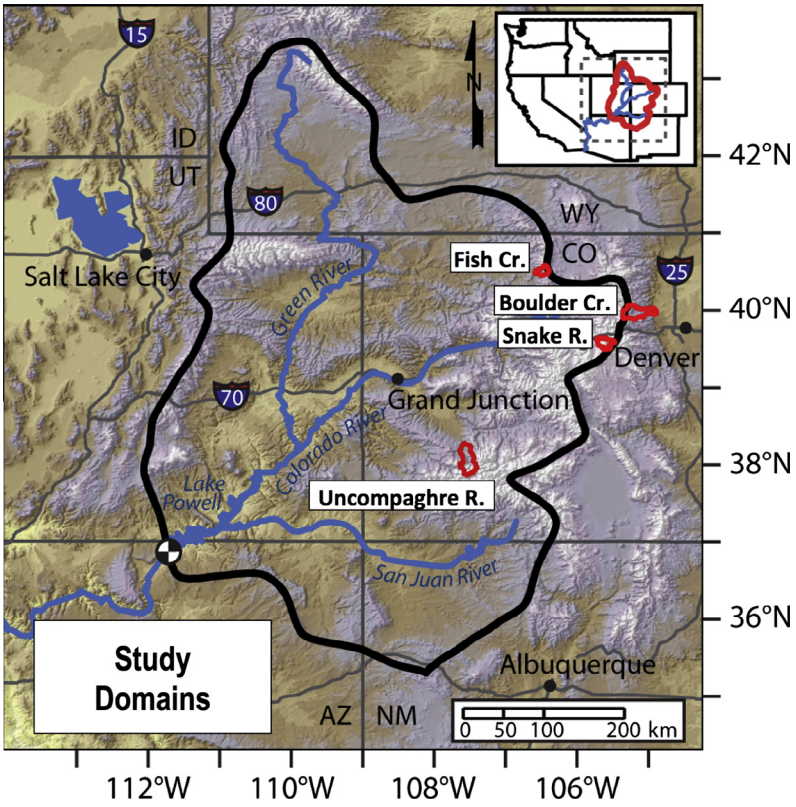

Fig. 1. Location of study catchments (red delineation) against elevation and the boundary (black) of the upper Colorado River Basin. (For interpretation of the references to color in this figure legend, the reader is referred to the web version of this article.)

Table 1
Characteristics of the four study catchments.

	Fish Cr.	Boulder Cr.	Snake R.	Uncompaghre R.
Gauge location	Steamboat springs	Orodell	Montezuma	Ridgeway reservoir
USGS I.D.	09238900	06727000	09047500	09146200
Drainage area (km^2)	67	274	150	386
Mean elevation (m)	2830	2770	3450	3125
Total relief (m)	1232	2397	1550	2422
Model grid length (m)	100	150	100	150
Coniferous area (%)[a]	49.9	66.0	48.6	35.2
Dominant geology (%)	Andesite (34.0%)	Glacial Drift (43.1%)	Intrusive Igneous (56.2%)	Metasedimentary and Metavolcanic (62.4%)
Mean annual precipitation 2000–2011 (mm)	1181	655	693	674

Meteorological Observation	Tower	Dry Lake	Niwot Ridge	Lake Eldora	Grizzly Peak	Dillon	Red Mtn. Pass	Idarado
Category	SNOTEL	SNOTEL	SNOTEL	SNOTEL	SNOTEL	Co-op	SNOTEL	SNOTEL
Elevation	3200	2560	3021	2957	3383	2763	3414	2987
Latitude (°N)	40.5374	40.5339	40.0352	39.9368	39.6333	39.6261	37.8918	37.9339
Longitude (°W)	106.6768	106.7813	105.5442	105.5896	105.8667	106.0353	107.7134	107.6755

[a] Represents the catchment area with land-cover susceptible to BB.

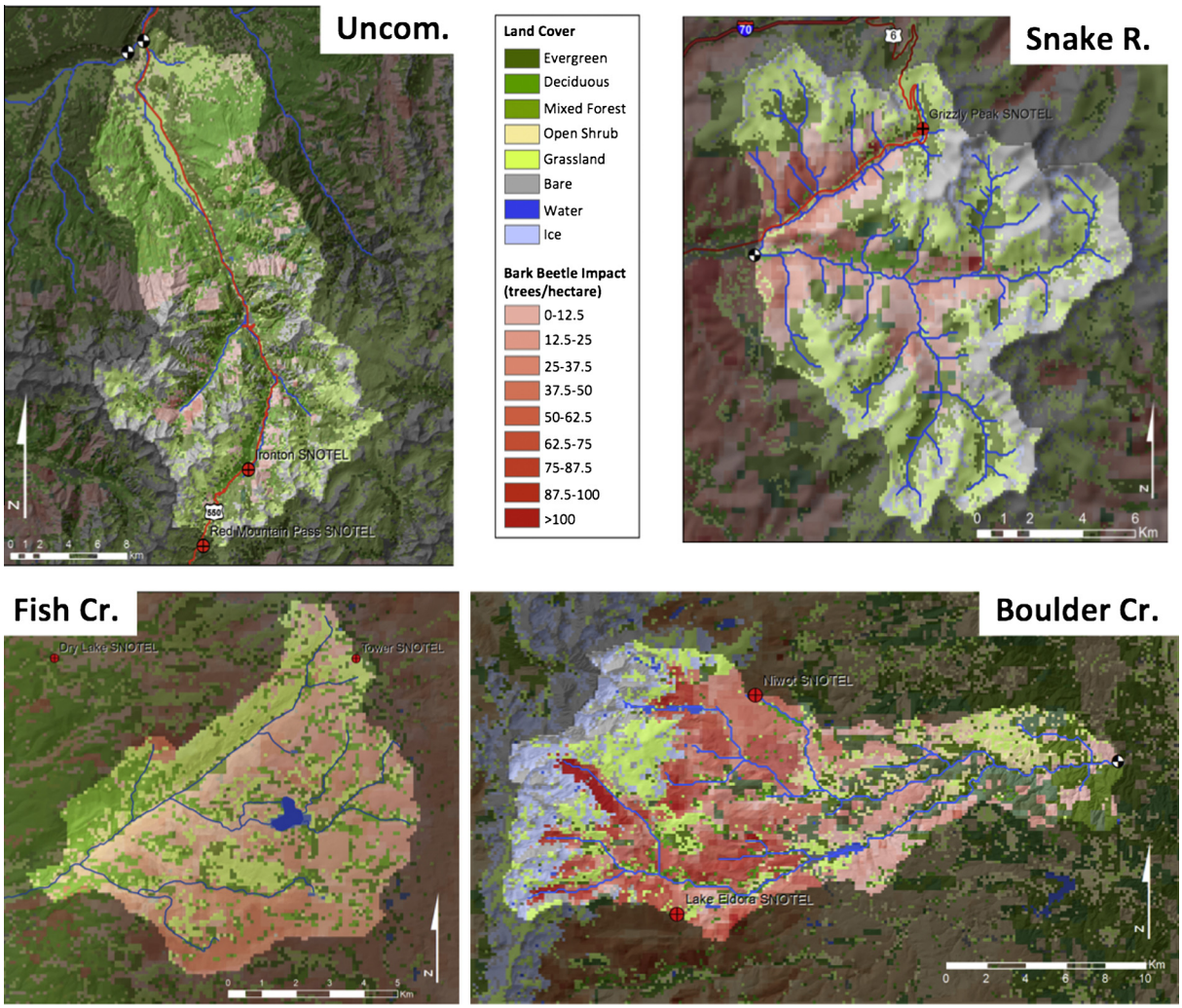

Fig. 2. Depiction of land cover classifications for each study catchment in addition to cumulative BB mortality as of 2011 based on the Ciesla (2006) aerial surveys; similar maps were used for each year in the range 2002–2011.

(1998), Bowling et al. (2000), and La Marche and Lettenmaier (2001). As such, the model allows for specification of monthly snow-free albedo and LAI for both overstory and understory layers (Table 2), as well as specification of rooting depths and stomatal resistance. In this way, the parameters needed for characterizing BB and dust-on-snow impacts are included the model.

2.3. Model characterization of BB impacts

To characterize the spatial extent and severity of BB impacts, tree mortality and BB phase maps were obtained from the United States Forest Service (USFS) aerial survey data created from annual flights conducted across the Southern Rocky Mountains

Table 2
DHSVM land cover classification and source information for parameter derivation via either pedo-transfer function or calibration.

Parameter	Pre-disturbance	Disturbance range	Source
Vegetation classification	National land cover database, 30 m spatial coverage	–	Fry et al. (2011)
Overstory Leaf Area Index (LAI) Needleleaf evergreen (–)	4.0	2.4–3.8[G]	Kaufmann et al. (1982) and Pugh and Small (2012)
Fractional coverage of forest canopy (–)	75%	0.61–0.72[G]	
Understory LAI (–)	0.5	1.5[RE]	MCD 15A2, 1 km spatial resolution, Buma et al. (2013)
Beetle kill severity	–	USFS polygons including trees per acre red and gray phases.	Ciesla (2006) and Meddens et al. (2011)
Change in needle-litter snow albedo (–)	–	1–9%[R]	Pugh and Small (2012)
Dust-on-snow albedo decay	Time dependent decay function	Based on low, moderate, extreme dust	Deems et al. (2013)

[G] Gray Phase.
[R] Red Phase.
[RE] Regeneration Scenario.

(Region 2, data available at: http://www.fs.usda.gov/main/r2/land-management/gis). Areas of mortality were mapped by trained observers, with density estimates of trees killed in the previous year (in terms of trees/acre) from a low altitude airplane (Ciesla, 2006). Accuracy depends on the scale of investigation and resolution, since estimates represent hand-drawn polygons on topographical maps. Point level accuracy was only 61.1% (in terms of mapped mortality to ground-truth data), but allowing for 500 m of error tolerance, accuracy improved to 78.6% (Johnson and Ross, 2006). Thus, these data are appropriate for watershed-scale investigations; however, limitations in the underlying data should be noted. The annual mapped polygons were reprojected to a 250 m raster using a nearest neighbor approach. The 250 m projection scale was chosen as a compromise between fine spatial resolution and representative accuracy of the mortality estimates, since finer spatial resolutions resulted in greater potential error rates. Given its comparatively longer duration of impact (>five years), gray phase exhibited consistent increases in both severity and spatial extent over time. Conversely, red phase prevalence was more variable, including decreases associated with conversion to gray phase on shorter time scales (<three years). The temporal history of red and gray phase severity and total-affected-area varied in each catchment. These complex temporal and spatial patterns of infestation challenge the detection of hydrologic responses in observed streamflow data (e.g. Bearup et al., 2014), necessitating our model sensitivity approach.

The two-layer DHSVM vegetation model was used to characterize BB forest impacts (Table 2) primarily through reductions to canopy LAI following the annual progression of BB impacts. LAI within DHSVM includes stem areas and effectively indexes canopy processes that (i) intercept precipitation, (ii) attenuate downwelling shortwave radiation and exchange longwave radiation with the understory, and (iii) modulate transpiration. Pre-disturbance LAI values for conifer species were assigned based on representative values for the Central Rocky Mountains (Kaufmann et al., 1982). The change in maximum annual LAI between green, red, and gray stages was examined using both satellite and in situ data—the ranges of disturbance values are listed in Table 2. Satellite estimates of canopy LAI before and after disturbance were obtained from MODIS (product MCD15A2, 1 km spatial resolution). Despite their relatively coarse resolution, MODIS LAI values matched well with in situ green and red phase estimates (Buma et al., 2013). However, during gray phase there was appreciably less correspondence between satellite and in situ data sources, due in large part to the mixing of overstory and understory LAI in the satellite imagery. Therefore, MODIS LAI was used only to verify the upper bound of LAI, but could not be used for more detailed estimates of LAI progression with increasing insect mortality. Relative changes in LAI from green-to-gray phases were

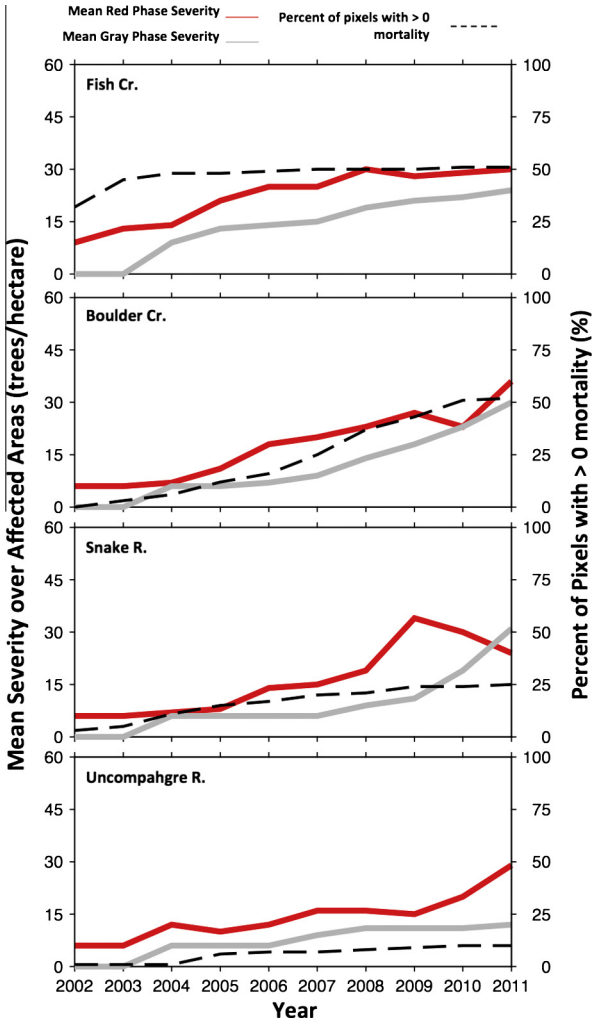

Fig. 3. Annual time series of BB mortality for each catchment from the USFS aerial surveys (Ciesla, 2006). Severity is shown in term of the mean trees per hectare in either red or gray phases (left vertical axis), and percentage of basin area with non-zero beetle mortality (right vertical axis). (For interpretation of the references to color in this figure legend, the reader is referred to the web version of this article.)

prescribed based on the local measurements of Pugh and Small (2013), who found an approximate 40% reduction in canopy LAI due to beetle impacts.

Beginning in 2002, DHSVM simulations for each water year were prescribed a different vegetation map according to BB disturbance severity from aerial survey data (e.g. Figs. 2 and 3) through subdividing impacted areas into discrete disturbance classes. Each disturbance class was assigned characteristics within the ranges listed in Table 2. Using binning increments of 5 dead trees per acre from the aerial data (12.5 dead trees per hectare) for both red and gray phases resulted in nine increments of severity for each phase and a combined total of 81 disturbed vegetation classes from which to linearly interpolate disturbance between values in Table 2 (8 red-phase disturbance classes + undisturbed red-phase = 9 red phase severities; 8 gray-phase disturbance classes + undisturbed gray-phase case = 9 gray phase severities, for a total of $9 \times 9 = 81$ combinations). For example, in the gray phase, the range of LAI is between 2.4 and 3.8, and canopy fractional coverage varies between 61% and 72%, such that a model pixel with the maximum (minimum) gray phase disturbance severity, i.e. >100 trees/ha ($\leqslant$12.5 trees/ha) would be assigned an LAI of 2.4 (3.8) and a fractional coverage of 61% (72%). For each class, BB-related changes were made to both the physical canopy structure, as well as the biological function of the canopy, e.g. transpiration. For the case of LAI, the maximum LAI (pre-disturbance) was obtained from Kaufmann et al. (1982), while the minimum (post-disturbance) of 40% reduction was from Pugh and Small (2013)—see Table 2 for further descriptions. Transpiration was reduced within each of the eight severity classes through scaling the vapor pressure deficit threshold at increments proportional to LAI-reductions. Pendall et al. (2010) observed a diminishing sensitivity of transpiration to vapor pressure deficit after beetle kill, with appreciable transpiration occurring only for the periods of greatest vapor pressure deficit. As stated above, canopy fractional coverage – largely affecting shortwave radiation transmittance – was reduced from 75% to 61% for gray phase following Pugh and Small (2012) based on the eight increments of disturbance severity.

The combination of fractional coverage and canopy LAI changes produced an initial estimate for the change in simulated canopy transmittance of approximately 5.5% between full-canopy and gray-phase BB scenarios. Canopy transmittance, T, is expressed as:

$$T = \frac{SW_{down,understory}}{SW_{down,canopy}} \quad (1)$$

where $SW_{down,understory}$ is the downwelling shortwave radiation reaching the understory and $SW_{down,canopy}$ is the downwelling shortwave incident upon the canopy. DHSVM was configured to compute transmittance following a simplified Beer's law formulation (Nijssen and Lettenmaier, 1999), such that:

$$SW_{down,understory} = SW_{down,canopy} \cdot exp^{k \cdot LAI} \quad (2)$$

where k is the radiation attenuation parameter, accounting for all canopy structural effects. Nijssen and Lettenmaier (1999) suggest that this parameter does not have a priori values, and recommend adjusting this parameter to match available observations. Bewley et al. (2010) manually adjusted k for the gray phase of a BB infestation in British Columbia, Canada, to more closely match observed changes in canopy transmittance. In this study, k was adjusted manually from 0.15 to 0.14, in order to increase simulated transmittance from 5.5% to the 6.8% reported value of Pugh and Small (2012). During snow covered periods, needle litter from red phase BB-impacts was parameterized through a reduction in understory snow albedo following the observational results of Pugh and Small (2012). A decrease in needle-related snow albedo of between 1% and 9% was applied for red phase only, based on the severity classes described above (e.g. the least severe disturbance, $\leqslant$12.5 trees/ha is assigned 1%, and the most severy, >100 trees/ha assigned 9%) and applied independent of any dust-on-snow related albedo changes.

Understory regeneration was simulated here through a single case considering maximum regeneration to represent a strong recovery end-member. The maximum regeneration LAI value was inferred by contrasting gray-stage plot data collected by Pugh and Small (2012) with concurrent MODIS LAI data over those same plots. Understory LAI for this scenario was estimated following the assumption that MODIS LAI identified during the gray phase (observed at 1.5) by Buma et al. (2013) was almost entirely due to understory vegetation, which was confirmed by Pugh and Small (2013), who visited each plot and confirmed gray stage conditions. Further, this regeneration of the understory is consistent with the findings of Romme et al. (1986), who found a threefold increase in growth for residual understory trees in the decade following overstory loss. An important caveat with this assumption is that the MODIS LAI is based on surface reflectance and biome-specific algorithms, coupled with pre-defined lookup tables that may not include the full range of vegetation reflectances observed by MODIS.

2.4. Model characterization of dust-on-snow impacts

Dust-on-snow was parameterized following Deems et al. (2013) in which the default DHSVM albedo decay curves (USACE, 1956) were adjusted to fit observations of broadband snow albedo time series in water years of low (LD), moderate (MD), and extreme dust (ED) forcing (Fig. 4). As discussed by Deems et al. (2013), these curves were derived using in situ observations from the Colorado River, noting the high tail of the ED curve during accumulation season was an artifact of the 2 years of extreme dust to fit those data (2009, 2010). It should be noted that during this time of year the impact of shortwave radiation on snowmelt is minimal due to lower sun angle and frequent storms, i.e. the tail of the accumulation curve is rarely experienced. Albedo decay curves prescribe an initial, clean snow albedo (0.85) for new snowfall, with subsequent albedo decrease with time following the snowfall event. Refreshing the snow albedo to 0.85 following new snow events represents a source of uncertainty, since it does not account for the extinction depth of radiation, where a thin layer of fresh snow may only

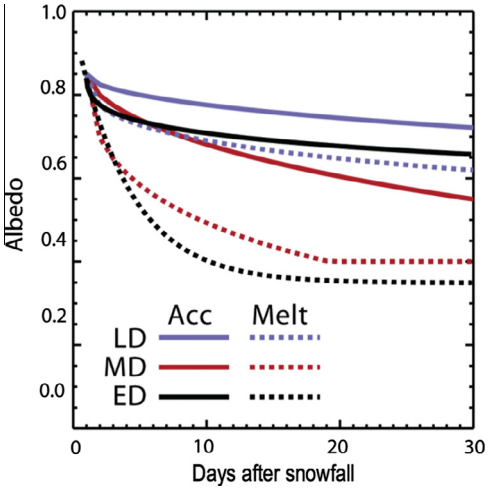

Fig. 4. Observation-based snow-albedo decay curves for moderate dust (MD), low dust (LD), and extreme dust (ED) deposition scenarios, where solid lines denote accumulation (Acc) season and dashed lines are for melt season (Melt) [adapted from Deems et al., 2013].

partially cover a darker underlying snowpack. Separate curves are used for accumulation and melt season, to accommodate more rapid albedo decay in the melt season due to snow grain metamorphism, which can be thought of as dry and wet snow albedos, respectively. Superposition of snow albedo modification was applied independently of forest disturbance effects on snow albedo, i.e. needle litter. Consistent with previous studies (Painter et al., 2012a; Deems et al., 2013) it is acknowledged here that prescribing a single dust scenario curve for each water year represents in important source of uncertainty and a physical simplification of the complex spatiotemporal dust deposition patterns, which in reality are associated with individual storm events. Table 3 shows the annual dust-on-snow severity time series used for each catchment, which defines the most realistic dust scenario, prescribed using a combination of qualitative in situ evidence (http://www.codos.org/#updates) as well as through the dust-on-snow radiative loading recorded from the MODIS Dust Radiative Forcing in Snow (MODDRFS) product (Painter et al., 2012b).

2.5. Soil parameter estimation

It has been suggested that for relatively steep mountain catchments, preferential flowpaths (e.g. macropores, pipes) and rapid subsurface flow are the dominant flow mechanisms, making the lateral soil conductivity, K_h, the most important soil parameter governing runoff generation in DHSVM (Whitaker et al., 2003). Experimental studies (e.g. Brooks et al., 2004) have shown that K_h is maximum near the soil surface and decreases exponentially with depth. A two-parameter analogue is followed in DHSVM, which is applied across three soil layers, with a total depth of between approximately 0.9 and 2.5 m, derived by local slop, upslope area, and elevation. Maximum K_h is assumed to occur at the land surface, with a decay parameter, f, that exponentially decreases K_h with depth, d, such that:

$$K_h(d) = K_{h,max} exp(-fd) \quad (3)$$

Therefore, the two critical calibration parameters were K_h and f. A simple Monte Carlo procedure was used to sample K_h and f within a range of 2 orders of magnitude for each catchment, which follows, since these parameters do not have a clear "default value", but are commonly estimated, or calibrated, in the literature. The range of K_h values were estimated as a function of the vertical soil hydraulic conductivity (K_v). Wigmosta et al. (1994) determined K_h from calibration as 100 times K_v; Vertessy et al. (1993) found optimal K_h values at 10 times K_v, while Brooks et al. (2004) experimentally found K_h to be 13.7 times K_v. Therefore K_h was varied between 2 and 200 times K_v during the search procedure. The range of f values were obtained from surveying the literature on DHSVM, with $f = 0.2$ (Wigmosta et al., 1994), $f = 1.4$ (Stonesifer, 2007), $f = 2.0$ (Whitaker et al., 2003), $f = 4.5$ (Thyer et al., 2004), such that f was allowed to vary from 0.1 to 10. Other soil parameters were estimated via soil texture relationships (references and details included in Table 4), including porosity, wilting point, and vertical hydraulic conductivity, K_v.

To select the final parameter values for f and K_h, an objective function minimizing differences between simulated and observed daily streamflow was selected following the daily Nash Sutcliffe efficiency (Nash and Sutcliffe, 1970), NSE:

$$\mathrm{NSE} = 1 - \frac{\sum_{t=1}^{n}(x_{s,t} - x_{o,t})^2}{\sum_{t=1}^{n}(x_{o,t} - \mu_o)^2} \quad (4)$$

where $x_{o,t}$ and $x_{s,t}$ are the observed and simulated values at each time-step, μ_o is the observed mean and n is the total number of time-steps, where 3-hrly model outputs were aggregated for daily comparison. An NSE value of 1 corresponds to a perfect model, while any value less than 0 describes a model that performs worse than simply using μ_o as the predictor. For top-performing simulations with similar NSE, the annual water balance ratio was used as a secondary metric (i.e. a component of NSE) to select among parameter sets.

During the parameter search, the dust-on-snow and vegetation parameters that were used corresponded to the prescribed annual time series of dust-on-snow severity (Table 3; Section 2.4) and BB disturbance (Fig. 3; Section 2.3). This simplification was made to keep the numerical problem tractable, given that extensive multiple-scenario calibrations are not the focus of this research. Foregoing additional calibration for each disturbance scenario allowed sensitivities to be reported from the disturbance mechanisms themselves (i.e. BB and dust-on-snow), rather than masking these responses by using different combinations of calibration soil parameters for each case.

Table 3
Temporal sequence of dust loading scenarios used for the 'time varying' case, where classifications of low (LD), moderate (MD), and extreme dust (ED) loadings follow the Deems et al., 2013 classification scheme.

	2000	2001	2002	2003	2004	2005	2006	2007	2008	2009	2010	2011
Fish	MD	MD	ED	MD	MD	LD	MD	MD	MD	MD	ED	LD
Boulder	LD	LD	ED	MD	MD	LD	MD	MD	MD	MD	ED	LD
Snake	LD	LD	ED	MD	MD	LD	MD	MD	MD	ED	ED	LD
Uncompahgre	MD	MD	ED	MD	MD	LD	MD	MD	MD	ED	ED	LD

Table 4
DHSVM model soil parameters distributed across each watershed, including those derived from pedo-transfer functions.

Input field	Description		Reference	
Soil classification	STATSGO 1:250,000 scale polygons applied over model grids.		Schwarz and Alexander (1995)	
Model Soil Parameters	Derived to model grid resolution using pedo-transfer functions		Zacharias and Wessolek (2007)	
Basin-specific parameter mean values	Fish Cr.	Boulder Cr	Snake R	Uncompahgre R
Vertical hydraulic conductivity K_v (10^{-4} m/s)	0.261	0.393	0.277	0.453
Porosity (–)	0.424	0.447	0.442	0.431
Wilting point (–)	0.126	0.131	0.121	0.103
[a]Horizontal hydraulic conductivity, K_h (10^{-4} m/s)	2.644	5.704	2.840	6.010
[a]Exponential decay parameter, f (–)	2.89	2.28	1.84	2.53

[a] Values obtained from calibration.

2.6. Meteorological input data

The meteorological data were obtained from the two observing stations in each basin and prepared following the recommendations of Livneh et al. (2014), which analyzed the same catchments as this study and focused on precipitation issues. In summary, gauge-observed daily precipitation, maximum and minimum temperatures were interpolated to each model grid from which other driving data for DHSVM were estimated. The major uncertainties in the meteorological data pertain to (i) precipitation undercatch, and (ii) the method for spatially distributing gauged precipitation. For complete details beyond the following description the reader is referred to Livneh et al. (2014).

Cold-season precipitation undercatch was minimized by contrasting recorded gauge precipitation with the snow pillow snow water equivalent (SWE) at SNOTEL stations. Discrepancies were resolved in favor of SWE, using a seven-day averaging window to account for jumps in the data. To distribute precipitation to all model grid cells within each catchment, the Parameter-elevation Regressions on Independent Slopes Model (PRISM; Daly et al., 1994) approach was ultimately selected after a comparison with a SWE reconstruction product (Molotch, 2009), interpolation, and an orographic precipitation rate. Despite the promise shown by the SWE reconstruction in distributing precipitation, it was most effective only when applied using the actual reconstructed SWE values, which ignores gauge precipitation magnitude and uses the gauge record only to temporally disaggregate precipitation, i.e. an estimate of precipitation frequency. Hence, it was elected to use the monthly PRISM product, to preserve gauge precipitation information in the analysis.

Beyond precipitation, DHSVM requires meteorological inputs including downwelling shortwave and longwave radiation, air temperature, and wind speed. Surface air temperature was obtained directly from the observation stations and lapsed with elevation (6.5 °C/km), whereas wind speed was obtained from the North American Regional Reanalysis (NARR; Mesinger et al., 2006). Similar to Livneh et al. (2014), the Mountain Microclimate Simulation Model (MT-CLIM) version 4.3 (Thornton et al., 2000) model was applied to estimate the full suite of inputs using only daily precipitation, minimum and maximum temperatures. Livneh et al. (2014) conducted comparisons of derived humidity, downwelling shortwave and longwave radiation with energy budget towers at Niwot Ridge Long Term Ecological Research site (Boulder Cr., http://culter.colorado.edu/NWT/) and Senator Beck Basin (Uncompaghre R; www.snowstudies.org). They computed small net biases, but larger mean absolute errors, suggesting that derived quantities represent long-term (i.e. >daily) forcing well, but would not capture larger sub-daily anomalies.

3. Results and discussion

The experimental results consist of three stages evaluating simulated hydrologic sensitivities of dust-on-snow, BB, and combined impacts, followed by a brief comparative analysis using observational evidence of BB impacts. The importance of experimental assumptions and uncertainties are weighed and a general discussion follows.

Model calibration was done for only the single most realistic dust (time-varying) and BB (annual disturbance maps) case for each basin, such that simulated sensitivities could be expressed near the range of observed hydrologic response. Supplemental Fig. A1 illustrates the impact of the calibration parameter search on streamflow for each basin, which highlights strengths and weaknesses in the modeling system. For the final calibrated model, daily NSEs of greater than 0.8 were obtained for three of the four catchments (NSE for Fish Cr: 0.85; Boulder Cr.: 0.76; Snake R.: 0.82; Uncompahgre R.: 0.82). Moriasi et al. (2007) categorize NSE values greater than 0.65 with 'good' hydrologic model performance and values greater than 0.75 as 'very good' on a monthly time scale, such that the daily values reported here would be considered 'very good' since NSE tends to be higher on monthly versus daily time steps for the annual time.

3.1. Dust-on-snow Impacts

The mean daily hydrographs of the low, moderate, and extreme DHSVM dust-on-snow scenarios (Fig. 4) reveal a strong influence of

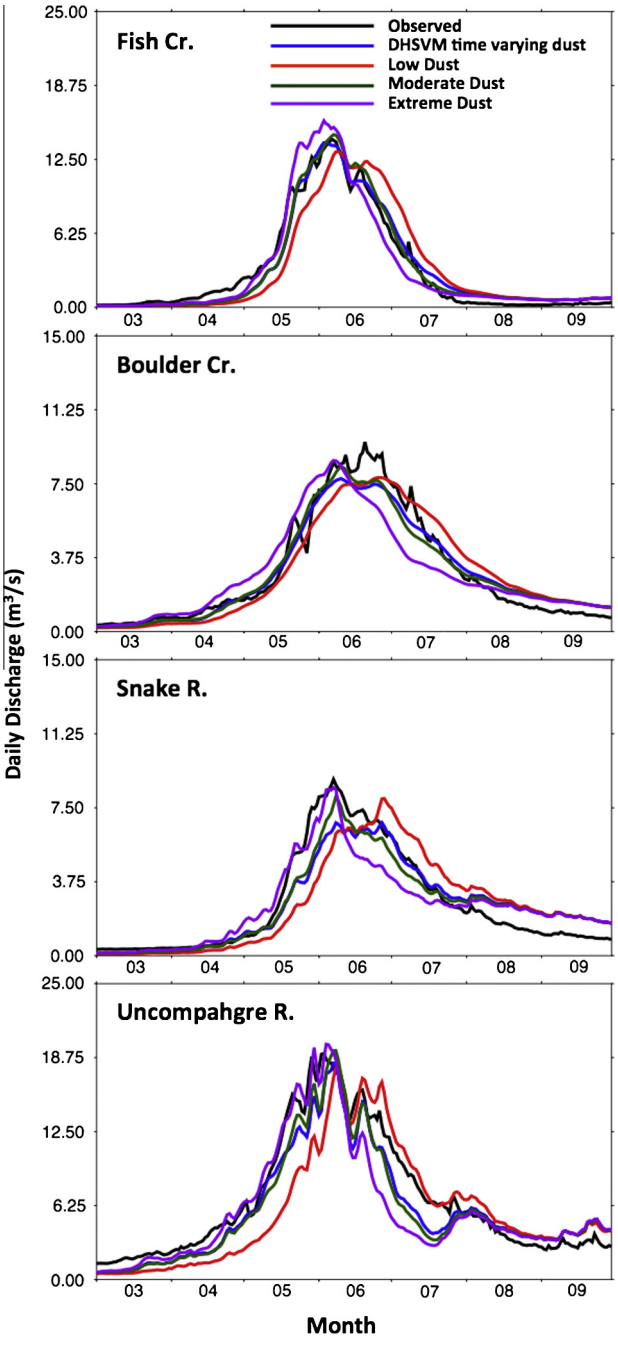

Fig. 5. Mean daily time-series (2000–2011) for the four study catchments including observed flows, three synthetic dust scenarios in which each scenario was run for all years of low, moderate, and extreme dust, as well as a 'time varying' dust scenario—i.e. the calibration case in which the most likely dust scenario was run for each year and basin, based on observational and remote sensing evidence described in Section 2.4.

Table 5
Streamflow and snow disappearance properties averaged over 2000–2011 water years for the 4 catchments prescribing low dust (LD), moderate dust (MD), and extreme dust (ED) for all years, contrasted against the 'time-varying' scenario in which the dust loading prescribed for each year was based on MODDRFS and in situ measurements (described in Section 2.4); the date at which 10% of peak SWE catchment-wide, Snow Disappearance-10 (SD-10), was selected as measure of basin-wide melt since some catchments have a small permanent snowpack in certain years; the NSE values reported are for the 'time-varying' case which was calibrated to observed daily streamflows.

		Centroid of streamflow (DOY)	Date of peak flow (DOY)	Water Yield (10^6 m^3)	SD-10 (DOY)
Fish	Time-varying	159.3	154.3	62.70	176.4
	LD	166.4	161.8	62.19	183.7
	MD	158.9	153.0	62.76	175.8
	ED	153.3	148.1	63.53	168.3
Boulder	Time-varying	169.9	170.4	57.24	185.8
	LD	176.3	173.8	57.04	194.3
	MD	168.1	166.3	57.35	183.2
	ED	159.4	155.9	58.19	175.9
Snake	Time-varying	168.3	173.5	56.10	166.4
	LD	175.9	183.8	56.32	173.3
	MD	166.4	174.7	55.68	163.9
	ED	158.2	163.8	56.75	157.8
Uncompahgre	Time-varying	150.6	160.3	141.11	164.9
	LD	163.0	171.7	138.42	179.7
	MD	150.4	162.7	140.54	164.8
	ED	145.3	157.3	143.12	159.7

dust-on-snow on snowmelt and peak runoff timing (Fig. 5). For these hypothetical cases, the same dust-on-snow scenario was run every water year, and compared to the calibrated 'time-varying' case, in which a different dust-on-snow scenario was selected each year based on observations and remote sensing, described in Section 2.4. Moving from the low to moderate to extreme dust-on-snow scenarios, timing of peak flow exhibits a clear shift as anticipated, with changes in peak timing date on the order of two to three weeks (13–20 days), where shifting from low to moderate dust had smaller variance in timing changes (8–9 days) than shifting from moderate to extreme (5–11 days). On average, the time-varying dust-on-snow case follows the moderate dust-on-snow case most closely, suggesting that moderate dust-on-snow may be a suitable estimate for average climatological conditions during the study period, in agreement with prior findings (Bryant et al., 2013; Deems et al., 2013).

Both the average date of peak flow and flow centroid (date at which 50% of annual flow has passed the stream gauge) move earlier into the year with increasing dust-on-snow, however they do not move monotonically with each dust-on-snow scenario (Table 5). Conversely, simulated water yield is much less sensitive to dust forcing and exhibited varying direction of sensitivity sign changes for one of the four catchments. Even the largest water yield sensitivities between dust scenarios, i.e. for the Uncompahgre R., are still relatively small (<2%). Although timing changes are consistent with previous research, the three catchments that show *increasing* water yield with increasing dust-on-snow are of opposite sign to the results of Painter et al. (2010) and Deems et al. (2013). Both of these studies were conducted at a much coarser model grid resolution (12 km grid cell) for the entire upper Colorado River basin. Catchment terrain geometry (e.g. slope and aspect) and vegetation cover may be responsible for this difference, resulting in varying sensitivity to dust-on-snow impacts on evapotranspiration and thus runoff volume among different headwaters catchments. DHSVM incorporates these features – slope and aspect – whereas the VIC model (Liang et al., 1994) used in the aforementioned studies assumes no within-grid aspect bias. DHSVM explicitly models the horizontal connectivity of adjacent grid cells for flow routing, allowing lower elevation cells to become saturated from headwater snowmelt, whereas the VIC model routing is a post-processing step. Despite this apparent disagreement with previous research, it is worth noting that none of the water yield changes shown here were found to be statistically significantly different from zero following a *t*-test ($p \leqslant 0.05$).

Since the primary action of dust-on-snow is on snowmelt rates, a metric of snow disappearance (SD) is tabulated in Table 5 describing the date at which 10% of post-peak snowpack remains catchment-wide (SD-10); this metric is less-sensitive to grid cells with permanent or late-lying snow patches than is the date of total melt-out, and thus is more representative of the seasonal ablation cycle. The date of SD-10 has consistent sensitivity to dust forcing across catchments, with heavier dust-on-snow years producing earlier average melt-out dates by between 15 and 20 days.

3.2. Bark veetle impacts

The primary drivers of hydrologic change from BB impacts are the cessation of root water uptake by infested trees and the reduction in live overstory canopy with increasing tree mortality. These effects should strongly reduce transpiration losses, and alter the surface energy balance, allowing greater solar input to soil, understory, and/or snow. DHSVM-simulated ET using time-varying

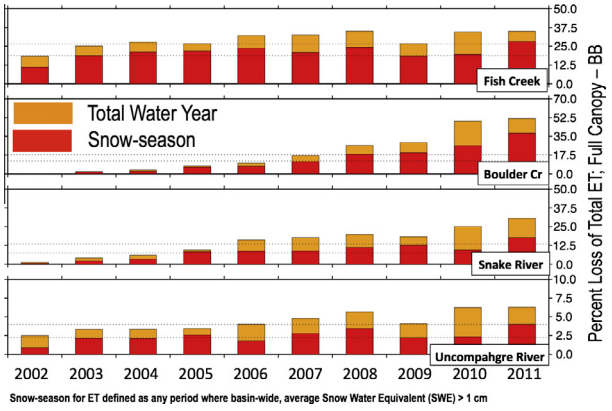

Fig. 6. Annual series (2002–2011) of BB sensitivities the four study catchments with the percentage decrease in ET shown as the difference between the pre-disturbance, i.e. full-canopy case, and the time-varying BB disturbance case described in Section 2.3. The total height of the bar denotes the total water year (i.e. the period from 1 Oct. to 30 Sep.), while differences with the contribution from the snow-season contribution presented (red bar) in front. The multi-year average values for total water year and snow-season are shown as a dotted lines. The distinction of the snow-season for ET was defined as any period where basin-wide, average SWE >1 cm, given the importance of snow cover to ET mechanisms. (For interpretation of the references to color in this figure legend, the reader is referred to the web version of this article.)

Table 6
Streamflow properties, 2002–2011, for the four catchments contrasting the time varying bark beetle (BB) impacts with a maximum regenerations scenario (BB-regen, detailed in Section 2.3), with an additional synthetic scenario in which DHSVM was run for all years with a pre-disturbance, i.e. full-canopy (no-BB); all cases consider the most realistic dust scenario, i.e. 'time-varying' and the BB case corresponds with the soil parameter calibration. Note, the major sensitivity term is water yield where BB sensitivities are roughly halved by the maximum regeneration scenario.

		Centroid of streamflow (DOY)	Date of peak flow (DOY)	Water yield (10^6 m^3)
Fish	BB	159.3	154.3	62.70
	BB-regen	159.0	153.5	59.28
	no-BB	158.5	152.7	55.15
Boulder	BB	169.9	170.4	57.24
	BB-regen	170.1	170.5	53.91
	no-BB	170.4	170.7	49.08
Snake	BB	168.3	173.5	56.10
	BB-regen	168.6	173.7	54.44
	no-BB	169.1	174.1	51.79
Uncompahgre	BB	150.6	160.3	141.11
	BB-regen	150.7	161.1	139.21
	no-BB	150.9	162.9	136.64

disturbance maps (described in Section 2.3) is compared against a control scenario, in which the pre-infestation vegetation cover, i.e. full-canopy, was run for the entire study period. The annual reductions in latent heating (ET) for each year appear to be strongly coupled to mortality extent (Figs. 3 and 6). The average annual decrease in ET across all basins is on the order of 15% with the greatest decreases in Fish Cr. and Boulder Cr., strongly tied to beetle kill severity and bearing strong semblance to the prescribed annual values of impacted catchment area (Fig. 3). The ET changes in Fig. 6 are partitioned into snow (>1 cm average catchment SWE) and snow-free ($\leqslant$1 cm average catchment SWE) seasons, since snow cover alters key latent heating mechanisms, such as free-surface evaporation and transpiration rate. The pairs of bars show a larger overall ET sensitivity in the snow season. It is worth noting that the snow season displayed in Fig. 6 lasts considerably longer than the warm season – between 6.5 and 8 months – suggesting that sensitivities are more balanced throughout the year. 2010 has a disproportionally high warm-season ET change due to BB, relative to other years. This is a result of lower winter precipitation (and snowpack) in 2010 with a BB mortality comparable to 2011; consequently a larger relative fraction of the water budget comes from snow-free season ET that year. Overall, the combination of model parametric assumptions and severity maps produced ET sensitivities that correspond to values of LAI intermediate to those reported by Kaufmann et al. (1982) and Pugh and Small (2012), since BB-related tree mortalities are heterogeneous over time and space. Importantly, BB-driven impacts on water yield are roughly halved when considering a maximum understory regeneration scenario (Table 6).

3.3. Combined BB and dust-on-snow impacts

The relative sensitivity of total water yield from BB far outweigh those due to dust-on-snow (Fig. 7), which exhibit their primary impact on streamflow timing. The timing of runoff peak and centroid are fairly insensitive to BB-impacts, shifting only modestly earlier in the year (<two days) in response to BB (Table 6). The exception in the direction of this shift is Fish Cr., where most of the BB impacts are on north facing slopes (established from the digital elevation model). The north facing aspect of BB impacts is important because reductions in canopy LAI from BB are associated with greater canopy openness. Increased canopy openness results in slightly larger SWE accumulation for all catchments. However, increased canopy openness also makes downwelling shortwave radiation (and aspect) of increasing importance on melt rates and subsequent peak flow and centroid timing. Therefore, because shortwave radiation is minimized on north-facing slopes, the north-facing BB-driven increases in peak-SWE in Fish Cr. outweigh increased solar exposure of the understory to dust-on-snow impacts. Overall, the modest BB-driven timing sensitivities (in either direction) suggest that any BB-related interactions with dust-on-snow-related timing changes should be minimal. In general, however, the effect of dust-on-snow is enhanced – earlier peak and centroid and earlier SD-10 – by BB. This is verified in Table 7, which shows modest changes in both peak flow and centroid timing when BB and dust-on-snow scenarios are combined. However, Fish Cr. is the exception, for the same reasons as described above. The relatively modest enhancements of BB on dust-on-snow are not entirely surprising, since the overall increase in canopy transmissivity between the full-canopy (no-BB) and BB scenarios is on the order of only 7%.

Modeling uncertainties together with BB and dust-on-snow parameterization assumptions collectively make drawing meaningful conclusions possible only for the most persuasive model results, namely that dust-on-snow increases melt rates and that

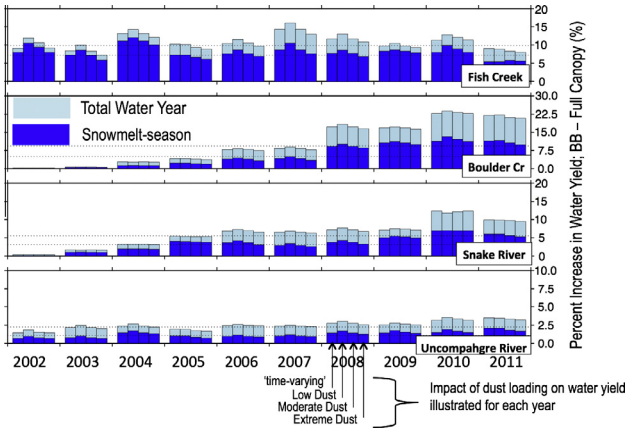

Fig. 7. Annual series (2002–2011) of combined BB and dust sensitivities for the four study catchments with the percentage increase in water yield shown as the difference between the pre-disturbance, i.e. full-canopy case, and the time-varying BB disturbance case. Differences are shown for the total water year (i.e. the period from 1 Oct. to 30 Sep.: full height of bar), with the snowmelt-season contribution presented (dark blue bar) in front, where the multi-year average values for total water year and snow-season are shown as a dotted lines. For consistency across basins, the distinction of the snowmelt-season for discharge was defined as the period between 1 March and 15 July based on manual examination of the onset and end of the snowmelt-driven observed hydrograph peak for each year. (For interpretation of the references to colour in this figure legend, the reader is referred to the web version of this article.)

Table 7
Same as Table 4, except compares bark beetle (BB) versus no bark beetle (no-BB) for all three dust scenarios; an additional column is added here showing catchment-wide average peak SWE magnitude.

		Centroid of streamflow (DOY)	Date of peak flow (DOY)	Water yield (10^6 m^3)	SD-10 (DOY)	Peak SWE (m)
Fish	no-BB LD	165.2	159.9	54.19	182.1	0.840
	LD	166.4	161.8	62.19	183.7	0.884
	no-BB MD	158.3	153.1	55.24	174.4	0.806
	MD	158.9	153.0	62.76	175.8	0.847
	no-BB ED	153.1	148.5	56.35	167.6	0.788
	ED	153.3	148.1	63.53	168.3	0.825
Boulder	no-BB LD	177.1	176.0	48.76	195.2	0.259
	LD	176.3	173.8	57.04	194.3	0.270
	no-BB MD	168.6	166.5	49.21	183.3	0.239
	MD	168.1	166.3	57.35	183.2	0.247
	no-BB ED	159.8	156.0	50.20	176.0	0.222
	ED	159.4	155.9	58.19	175.9	0.229
Snake	no-BB LD	176.9	184.3	51.92	174.5	0.256
	LD	175.9	183.8	56.32	173.3	0.266
	no-BB MD	167.3	175.4	51.40	164.3	0.230
	MD	166.4	174.7	55.68	163.9	0.237
	no-BB ED	159.1	163.8	52.50	157.9	0.222
	ED	158.2	163.8	56.75	157.8	0.228
Uncompahgre	no-BB LD	163.3	171.7	133.80	179.8	0.234
	LD	163.0	171.7	138.42	179.7	0.237
	no-BB MD	150.7	165.3	136.08	165.0	0.210
	MD	150.4	162.7	140.54	164.8	0.213
	no-BB ED	145.5	160.8	138.75	159.8	0.206
	ED	145.3	157.3	143.12	159.7	0.209

Table 8
Net hydrologic impacts of BB and dust-on-snow (DOS) from the four study catchments, with causal explanations; "*N*/*C*" denotes no consistent change.

	Water yield	Low flow	Peak flow timing	Peak SWE
BB	*Increase:* Greater snow accumulation from reduced canopy sublimation; Greater warm-season flow due to reduced transpiration	*Increase:* Reduced warm-season transpiration	*N*/*C*	*Increase:* Reduced canopy interception and sublimation
Dust-on-snow	*N*/*C*	*N*/*C*	*Earlier:* Greater net solar radiation enhances snowmelt	*N*/*C*
Combined	*Increase:* Due to BB effects	*Increase:* Due to BB effects, but reduced by faster snowmelt from DOS	*Earlier:* Due to DOS effects; small enhancement from BB-reduced canopy shading	*Increase:* Due to BB effects

BB may increase water yield. In the absence of notable interaction, the net hydrologic impacts from BB and dust-on-snow are summarized in Table 8, for which the BB sensitivities largely follow those illustrated by Pugh and Gordon (2012). The level of environmental complexity in drawing such conclusions was the motivation for employing a model here, since the size of the hydrologic signal from these disturbances relative to inter-annual climatic variability is often too small and noisy to discern from observations alone. Below, the size of the BB-disturbance signal is quantified and its significance is explored strictly through observational data.

3.4. Observational evidence of BB sensitivity

To explore observational evidence for changes in hydrologic fluxes caused by BB, the results in this section are presented using a simple water balance approach. The observed runoff coefficient, R_c, was computed on an annual basis:

$$R_c = \frac{Q}{P} \tag{5}$$

where Q is observed annual discharge (USGS stations listed in Table 1) and P is total annual observed precipitation (Section 2.6). Based on the review of the literature, we posit that BB mortality reduces ET, thereby increasing R_c through increases in Q. Since both P and Q can be observed and BB-related tree mortality has been remotely-sensed, the hypothesis is that a BB-induced runoff signal should be detectable through contrasting R_c against cumulative BB mortality. BB sensitivity in this context may be understood best through considering the terms in the land-surface water budget:

$$P = Q - ET - \Delta S \tag{6}$$

where ΔS is the change in inter-annual carryover storage, i.e. between surface water and groundwater. Substituting (6) into (5) and rearranging produces:

$$R_c = 1 + \frac{(ET + \Delta S)}{P} \tag{7}$$

The assumption here is that R_c is sensitive to BB through changes in ET. This follows since discharge, Q, is a remainder (Langbein, 1949), which can only begin after abstractions of water due to ET, interception storage, ΔS, and depression storage have occurred (Ratzlaff, 1994). Although Q is directly sensitive to P, ET and ΔS are assumed to be less sensitive to P, but rather more sensitive to environmental demand terms like vapor pressure deficit and antecedent soil moisture. Vlčková et al. (2009) showed that R_c is insensitive to groundwater level – a component of ΔS – whereas a number of studies have linked R_c to land cover, specifically changes in forest cover (e.g. Sun et al., 2006; Andréassian, 2004; Brown et al., 2005), a quantity which is directly influenced by BB. Bearup et al. (2014) recently used observed isotope data to calculate BB-driven transpiration losses and confirmed subsequent changes in streamflow generation

processes, suggesting both terms in the numerator of the rightmost term in Eq. (7) would be altered by BB.

To objectively quantify the spatial extent of BB impacts, the data set of Meddens et al. (2011) was used. This data set is derived from the same aerial survey data (Ciesla, 2006) described in Section 2.3. However, a key distinction for the Meddens et al. (2011) data is that mortality is expressed in terms of hectares of affected forest per square kilometer, rather than broken into red- and gray-phases as was the case for the Ciesla (2006) data. This value of mortality could be interpreted as a percentage, since 100 ha comprise a square kilometer, however, strictly speaking it is not the case.

A potential systematic bias in R_c response to BB is anticipated to occur as a function of precipitation variability (i.e. dry years having proportionately less runoff than wet years), so we de-trended the annual R_c series by precipitation. The leftmost two panels in Fig. 8 reveal a positive correspondence between R_c and cumulative BB-mortality for BB mortality expressed both in terms of % of catchment area, as well as % of intra-catchment in coniferous forest within each catchment. Despite weak to moderate correlations, the data have a high degree of scatter. Three of the four catchments (excluding the Uncompahgre R) have line slopes that are significantly different from zero at a threshold of $p \leqslant 0.05$, whereas none of these are significant at $p \leqslant 0.01$. It follows that the Uncompahgre line slope was not significant, as it has the smallest BB disturbance fraction among the catchments. The relationship between P and R_c (second column from the right, Fig. 8) exhibits moderate correlations and positive slopes across catchments. For Fish Cr. and the Uncompahgre R. the slope of these lines is significantly different from zero ($p \leqslant 0.01$), suggesting that de-trending R_c by P, i.e. considering the R_c-residual, will reduce unintended biases in a BB-sensitivity estimate. First-order Q–P dependencies were removed by plotting the residual from the P–R_c curve against cumulative BB mortality in the leftmost column of Fig. 8. Despite a positive slope in the residual plots for each catchment, a large scatter exists with weak correlations, indicating a positive, but statistically insignificant relationship between BB and Q for all catchments.

The large scatter in these relationships highlights the motivation for employing a hydrologic model to quantify BB impacts. In order to contrast the results from Fig. 8 against the DHSVM sensitivities, the slope of the line for the R_c-residual vs. BB plots represents a conservative estimate of catchment hydrologic sensitivity to BB mortality. If the Uncompahgre R. is excluded due to its small overall mortality, then the de-trended runoff

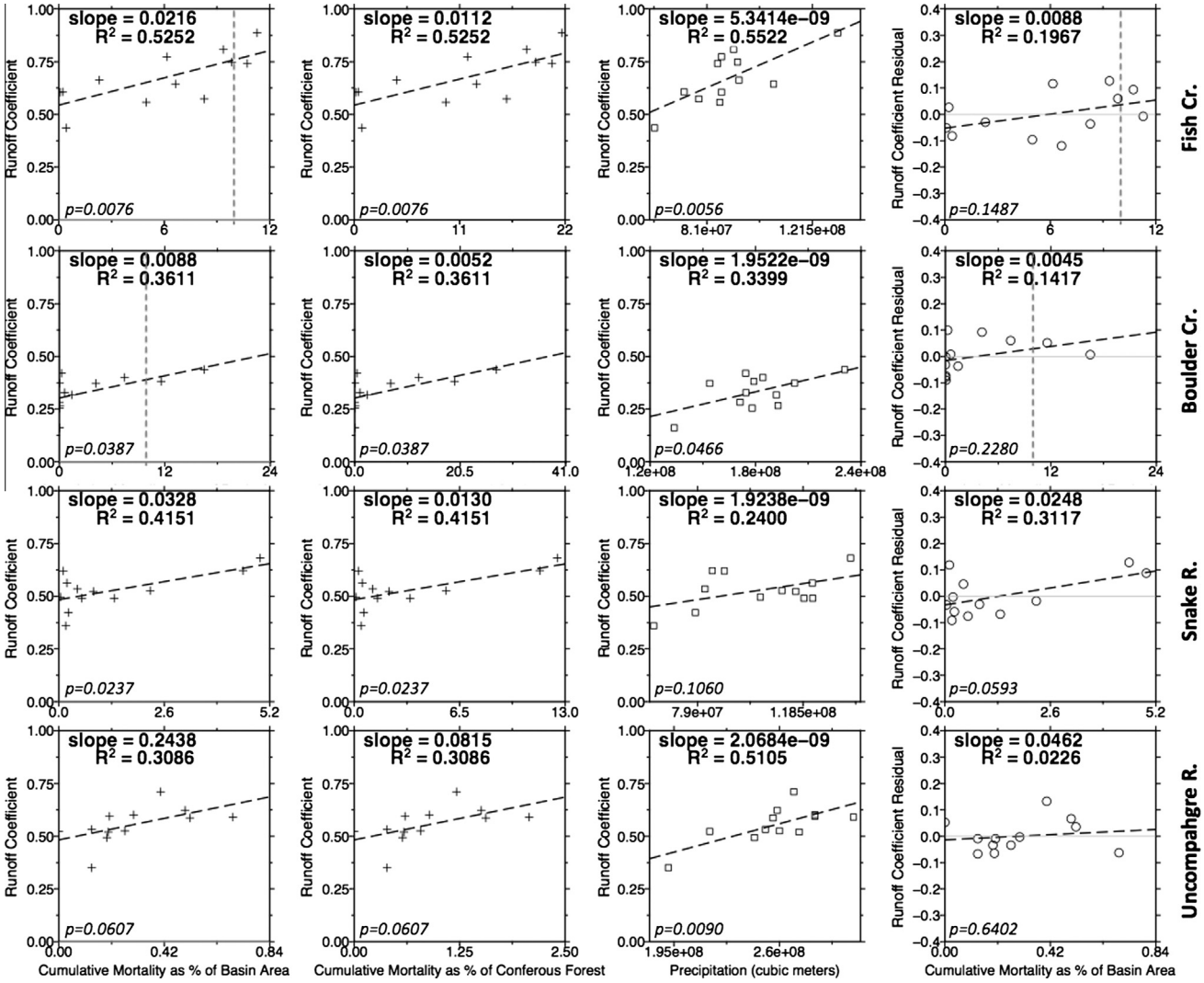

Fig. 8. Comparison of annual runoff coefficient, R_c, versus (leftmost) cumulative BB mortality as a percentage of catchment area, (second from left) cumulative BB mortality as a percentage of intra-catchment coniferous forested area, (second from right) annual precipitation, P, volume, whereas the rightmost plot is essentially a repeat of the leftmost panel, except the R_c residual is plotted, i.e. the residual term from the P–R_c line is shown to remove first-order dependencies. The slope of each line, the statistical p-value, and the square of the Pearson correlation coefficients, R, are listed, revealing consistent positive slopes between BB and R_c, but extremely large scatter. Vertical dashed lines demark 10% mortality per basin area. Note only Fish Cr. and Boulder Cr. exceed this threshold.

coefficient relationships suggest runoff volume sensitivity on the order of approximately 4–25% per 10% catchment-wide mortality. If we further focus only on the catchments that *actually* experienced more than 10% mortality, then the sensitivity falls to between 4% and 9% increase in runoff per 10% mortality. This result agrees reasonably with the DHSVM sensitivities that are roughly 8–13% and 4–8% for the same catchments with and without under-canopy regeneration, respectively.

3.5. Discussion

In the present study, the level of forest mortality was relatively small compared with other disturbance studies exploring impacts of clear-cutting and fire. Brown et al. (2005) reviewed 94 paired watershed studies and concluded that reductions in forest biomass of less than 20% apparently cannot be detected from measuring streamflow. Despite having less than 20% mortality in this study (Fig. 8), the sign of BB-related increases in water yield are consistent with early paired-catchment studies (Bethlahmy, 1975; Potts, 1984). However, the magnitudes of water yield changes in this study are much more modest than the aforementioned studies, also with considerable noise in the observed signal. In a model-based analysis, Rudolph (2012) found between a 1% and 10% increase in water yield using a hydrologic model (VIC) for the North Platte basin, assuming between 16% and 40% mortality rates. Smaller sensitivities were found by Somor (2010), who used a multiple-linear-regression (MLR) method to estimate pre-and-post BB outbreak for eight catchments in Colorado, finding no statistical change in water yield in seven out of eight catchments. The only statistically significant change in that case was negative for single catchment, which experienced record warm temperatures, although Somor (2010) ultimately concluded the MLR model to be an incomplete representation of the physical system. Similarly, Guardiola-Claramonte et al. (2011) reported decreases in water yield (i.e. opposite in sign to the present study) for semi-arid catchments with forest mortality in areas generally further south and more arid that our four study catchments. Despite the fact that they were not able to isolate the cause of the streamflow decrease, they cite both increases in understory vegetation and solar radiation reaching the understory – both of which are associated with enhanced soil and understory ET fluxes and reductions in overland flow. It follows that Carver et al. (2009) found overland flow not to be the dominant streamflow mechanism over BB impacted watershed areas in British Columbia. Altogether, considerable disagreement in water yield sensitivity exists among BB-disturbance studies, suggesting both an incomplete representation of the physical system, as well as site-specific factors dominating system response. The sign and magnitude of the current results ultimately fall within the reported range of sensitivities.

The impact of BB on cold-season processes shown in this study was expressed through reduced canopy interception and subsequent reduction in canopy sublimation processes, leading to increased water availability at the land surface. This mechanism has been confirmed in two modeling studies (Alila et al., 2009; Bewley et al., 2010) in British Columbia and through observational evidence (Biederman et al., 2014) in a set of study locations just east of the continental divide in Wyoming. However, in the latter observational study sites, the overall peak SWE for BB vs. non-BB stands were not statistically different from each other. Biederman et al. (2014) suggest a compensatory factor of increased subcanopy snow sublimation in BB-stands due to higher sub-canopy wind speeds. This compensatory behavior was not explicitly simulated by DHSVM representing a potential caveat in the analysis. A major reason for this was that the aerodynamic attenuation in the model is controlled by canopy height and trunk spacing, which both remained constant in the BB scenarios, similar to the model settings used by Bewley et al. (2010). A further simplification is from the coarse wind data (NARR), which despite capturing temporal variability in wind speed, do not adequately represent the intra-catchment distribution of wind with topography. However, it is worth noting that the Biederman et al. (2014) stands are located near the continental divide in Wyoming, in areas commonly experiencing very high winds and gusty conditions, which may provide the necessary energy to facilitate sub-canopy sublimation rates capable of compensating for BB-driven reductions in canopy sublimation.

Although management strategies in response to BB-infestations were not discussed here, one potential strategy has been to 'clear-cut' BB-infested stands, as was the case in parts of Grand County, CO (Lockwood, 2012). To this end, a 'clear-cut' scenario was considered during the course of this research. The simulated hydrologic response for clear-cut scenarios is notably different than for forested cases (both with and without BB) and as such, makes a direct comparison complicated. Clear-cut hydrology in the four catchments consistently produced larger peak snowpacks and marked increases in water yield for all dust-on-snow scenarios – similar in sign to the peak SWE changes in Table 7 between no-BB to BB, but with peak magnitudes on the order of 10–20% larger than the BB case. In light of the larger cold-season water storage, peak flows and flow centroids generally occurred slightly later than for forested cases (both BB and no-BB). Relative to the forested cases, the impact of increased melt rates from the lack of canopy attenuation of shortwave radiation and higher understory wind speeds were collectively outweighed by larger SWE accumulations associated with clear-cutting.

The results from the dust-on-snow sensitivities indicate earlier snowmelt-driven streamflow, consistent with previous studies looking at streamflow changes (Painter et al., 2010; Deems et al., 2013) and point snowmelt simulations (Skiles et al., 2012). The direct relationship between dust-on-snow and snowmelt rate have been confirmed observationally (Painter et al., 2012a), suggesting that this finding is robust. There is greater uncertainty in the impact of dust-on-snow on overall water yield as compared with flow timing, since there are substantially more complex and numerous mechanisms involved in the transmission of earlier and more rapid snowmelt to the river channel. These influences include transit time (a function of catchment size and geometry), vegetation cover (forested versus unforested), aspect, length of the warm-season and choice and scale of hydrologic modeling system. Given these complexities, it is not entirely surprising that the magnitude and even sign of the water yield versus dust-on-snow sensitivities are not in full agreement with prior, basin-scale studies (Painter et al., 2010; Deems et al., 2013). Those studies were geared toward gaining a broad-scale understanding (12 km pixel size) of the processes affecting the entire upper Colorado River basin (278,070 km^2). At finer scales, individual catchment terrain, geometry, vegetation coverage, climate, and dust forcing are likely to induce variation from the full-basin hydrologic response. Finally, the assumption of spatially homogenous dust deposition curves (e.g. published by Painter et al., 2010; Deems et al., 2013) represents an important source of uncertainty that could affect both timing and magnitude of snowmelt runoff. We recommend future work be directed toward further refinements that are beyond the scope of this analysis, to explicitly resolve the impacts of scale, slope, aspect, surface winds, dust spatiotemporal heterogeneity, and model selection on dust-on-snow water yield sensitivities.

4. Conclusions

Annual vegetation disturbance information was used to drive a distributed hydrologic model and to quantify impacts of forest

disturbance on hydrology. Overall, the simulations suggest increases in water yield due to bark beetle (BB) mortality of between 8% and 13%, dependent on catchment. However, using a maximum understory regeneration scenario roughly halved these sensitivities.

For the four snowmelt-dominated study catchments considered in this analysis, dust-on-snow has a marked impact on streamflow timing, with increasing dust forcing associated with earlier peak timing on the order of two to three weeks (13–20 days) and earlier snow disappearance of similar temporal sensitivity (15–20 days). Changes to water yield were modest and statistically insignificant, and their sign were not consistent among dust-on-snow scenarios for all catchments, which in one case, were of opposite sign to those reported by previously published simulations at much coarser scales.

Combinatory impacts between dust-on-snow and BB appear to be relatively minimal, with the former primarily affecting flow timing and the latter impacting water yield. The main interaction of BB with dust-on-snow impacts is through increased transmittance of shortwave radiation reaching the snow surface, causing a slightly larger onset of snowmelt-driven streamflow.

A purely observational analysis was conducted, suggesting consistent but statistically insignificant increases in water yield associated with BB on the order of between 4% and 9% change for 10% catchment mortality. Given the range of observational uncertainties and model assumptions, it is recommended that future research be focused on the importance of model selection and micrometeorology; on dust-on-snow, BB, and combined sensitivities.

Acknowledgements

We would like to acknowledge Leanne Lestak for her GIS assistance. This research was funded by the NOAA Climate Program Office through the Western Water Assessment RISA at CIRES, University of Colorado-Boulder. The data used in this analysis can be obtained by contacting the corresponding author directly.

Appendix A. Supplementary material

Supplementary data associated with this article can be found, in the online version, at http://dx.doi.org/10.1016/j.jhydrol.2015.01.039.

References

Alfaro, R.I., Campbell, R., Vera, B., Hawkes, B., Shore, T.L., 2004. Dendroecological reconstruction of mountain pine beetle outbreaks in the Chilcotin Plateau of British Columbia. In: Shore, T.L., Brooks, J.E., Stone, J.E. (Eds.), Challenges and Solutions: Proceedings of the Mountain Pine Beetle Symposium. Kelowna, British Columbia. October 30–31, 2003, pp. 245–256. Natural Resources Canada, Canadian Forest Service, Pacific Forestry Centre, Victoria, British Columbia, Information Report BC-X-399, 298 p.

Alila, Y., Bewley, D., Kuras, P., Marren, P., Hassan, M., Luo, C., Blair, T., 2009. Effects of Pine Beetle Infestations and Treatments on Hydrology and Geomorphology: Integrating Stand-level Data and Knowledge into Mesoscale Watershed Functions. Natural Resources Canada, Canadian Forest Service, Pacific Forestry Centre, Victoria. Mountain Pine Beetle Working Paper 2009-06.

Andréassian, V., 2004. Waters and forests: from historical controversy to scientific debate. J. Hydrol. 291 (1), 1–27.

Bearup, L.A., Maxwell, R.M., Clow, D.W., McCray, J.E., 2014. Hydrological effects of forest transpiration loss in bark beetle-impacted watersheds. Nat. Clim. Chan. 4 (6), 481–486.

Bentz, B.J., Allen, C.D., Ayres, M., Berg, E., Carroll, A., Hansen, M., Hicke, J., Joyce, L., Logan, J., MacFarlane, W., MacMahon, J., Munson, S., Negron, J., Paine, T., Powell, J., Raffa, K., Régnière, J., Reid, M., Romme, W., Seybold, S., Six, D., Tomback, D., Vandygriff, J., Veblen, T., White, M., Witcosky, J., Wood, D., 2009. In: Bentz, B.J. (Ed.), Bark Beetle Outbreaks in Western North America: Causes and Consequences. Univ. of Utah Press, Chicago, IL (ISBN: 978-0-87480965-7, 42).

Bethlahmy, N., 1974. More streamflow after a bark beetle epidemic. J. Hydrol. 23 (3–4), 185–189.

Bethlahmy, N., 1975. A Colorado episode: beetle epidemic, ghost forests, more streamflow. Northwest Sci. 49 (2), 95–105.

Bewley, D., Alila, Y., Varhola, A., 2010. Variability of snow water equivalent and snow energetics across a large catchment subject to Mountain Pine Beetle infestation and rapid salvage logging. J. Hydrol. 388, 464–479.

Biederman, J.A., Brooks, P.D., Harpold, A.A., Gochis, D.J., Gutmann, E., Reed, D.E., Pendall, E., Ewers, B.E., 2014. Multiscale observations of snow accumulation and peak snowpack following widespread, insect-induced lodgepole pine mortality. Ecohydrology 7, 150–162. http://dx.doi.org/10.1002/eco.1342.

Boon, S., 2007. Snow accumulation and ablation in a beetle-killed pine stand, northern Interior British Columbia, BC. J. Ecosyst. Manage. 8 (3), 1–13.

Bowling, L.C., Storck, P., Lettenmaier, D.P., 2000. Hydrologic effects of logging in western Washington, United States. Water Resour. Res. 36, 3223–3240.

Brooks, E.S., Boll, J., McDaniel, P.A., 2004. A hillslope-scale experiment to measure lateral saturated hydraulic conductivity. Water Resour. Res. 40 (4).

Brown, A.E., Zhang, L., McMahon, T.A., Western, A.W., Vertessy, R.A., 2005. A review of paired catchment studies for determining changes in water yield resulting from alterations in vegetation. J. Hydrol. 310 (1), 28–61.

Bryant, A.C., Painter, T.H., Deems, J.S., Bender, S.M., 2013. Impact of dust radiative forcing in snow on accuracy of operational runoff prediction in the Upper Colorado River Basin. Geophys. Res. Lett. 40 (15), 3945–3949. http://dx.doi.org/10.1002/grl.50773.

Buma, B., Pugh, E.T., Wessman, C.A., 2013. Effect of the current major insect outbreaks on decadal phenological and LAI trends in southern Rocky Mountain forests. Int. J. Remote Sens. 34 (20), 7249–7274. http://dx.doi.org/10.1080/01431161.2013.817717.

Carrasco, P., Hamlet, A.F., 2010. Fine Scale Hydrologic Model Implementation and Fine-scale/Macro-scale Model Inter-comparison Study. Final Report for the Columbia Basin Climate Change Scenarios Project, Climate Impacts Group, Center for Science in the Earth System, Joint Institute for the Study of the Atmosphere and Ocean, University of Washington, Seattle (Chapter 6).

Carver, M., Weiler, M., Stahl, K., Scheffler, C., Schneider, J., Naranjo, J.A.B., 2009. Development and Application of a Peak Flow Hazard Model for the Fraser Basin (British Columbia). Report to Natural Resources Canada (Canadian Forest Service), Victoria, BC, Project #7.29, 37 p.

Ciesla, W.M., 2006. Aerial Signatures of Forest Insect and Disease Damage in the Western United States, USDA Forest Service, Forest Health Technology Enterprise Team FHTET-01-06.

Cline, D.W., 1997. Snow surface energy exchanges and snowmelt at a continental, midlatitude Alpine site. Water Resour. Res. 33 (4), 689–701.

Collins, B.J., Rhoades, C.C., Hubbard, R.M., Battaglia, M.A., 2011. Tree regeneration and future stand development after bark beetle infestation and harvesting in Colorado lodgepole pine stands. For. Ecol. Manage. 261 (11), 2168–2175.

Daly, C., Neilson, R.P., Phillips, D.L., 1994. A statistical–topographic model for mapping climatological precipitation over mountainous terrain. J. Appl. Meteorol. 33, 140–158.

Deems, J.S., Painter, T.H., Barsugli, J.J., Belnap, J., Udall, B., 2013. Combined impacts of current and future dust deposition and regional warming on Colorado River Basin snow dynamics and hydrology. Hydrol. Earth Syst. Sci. 17 (11), 4401–4413. http://dx.doi.org/10.5194/hess-17-4401-2013.

Dennison, P.E., Brunelle, A.R., Carter, V.A., 2010. Assessing canopy mortality during a mountain pine beetle outbreak using GeoEye-1 high spatial resolution satellite data. Remote Sens. Environ. 114 (11), 2431–2435.

Fry, J., Xian, G., Jin, S., Dewitz, J., Homer, C., Yang, L., Barnes, C., Herold, N., Wickham, J., 2011. Completion of the 2006 national land cover database for the conterminous united states. Photogramm. Eng. Remote Sens. 77 (9), 858–864.

Guardiola-Claramonte, M., Troch, P.A., Breshears, D.D., Huxman, T.E., Switanek, M.B., Durcik, M., Cobb, N.S., 2011. Decreased streamflow in semi-arid basins following drought-induced tree die-off: a counter-intuitive and indirect climate impact on hydrology. J. Hydrol. 406 (3), 225–233.

Hicke, J.A., Jenkins, J.C., 2008. Mapping lodgepole pine stand structure susceptibility to mountain pine beetle attack across the western United States. For. Ecol. Manage. 255, 1536–1547.

Hicke, J.A., Logan, J.A., 2009. Mapping whitebark pine mortality caused by a mountain pine beetle outbreak with high spatial resolution satellite imagery. Int. J. Remote Sens. 30, 4427–4441.

Hubbard, R.M., Rhoades, C.C., Elder, K., Negron, J., 2013. Changes in transpiration and foliage growth in lodgepole pine trees following mountain pine beetle attack and mechanical girdling. For. Ecol. Manage. 289, 312–317.

Johnson, E., Ross, J., 2006. Technical Report R2-06-08; USDA Forest Service Rocky Mountain Region Forest Health Aerial Survey Accuracy Assessment 2005 Report. USDA Forest Service Rocky Mountain Region Renewable Resources PO Box 25127 Lakewood, CO 80225-01.

Kaufmann, M.R., Edminster, C.B., Troendle, C.A., 1982. Leaf Area Determinations for Subalpine Tree Species in the Central Rocky Mountains. USDA Forest Service, Rocky Mtn. For. And Range Exp. Sta. Res., Paper RM-238, 7p.

La Marche, J.L., Lettenmaier, D.P., 2001. Effects of forest roads on flood flows in the Deschutes river, Washington. Earth Surf. Proc. Landforms 26, 115–134.

Langbein, W.B., 1949. Annual Runoff in the United States, U.S. Geological Survey Circ, vol. 52, 14 pp.

Lewis, K.J., Hartley, I.D., 2006. Rate of deterioration, degrade, and fall of trees killed by mountain pine beetle, BC. J. Ecosyst. Manage. 7 (2), 11–19.

Liang, X., Lettenmaier, D.P., Wood, E.F., Burges, S.J., 1994. A simple hydrologically based model of land surface water and energy fluxes for general circulation models. J. Geophys. Res. Atmos. (1984–2012) 99 (D7), 14415–14428.

Livneh, B., Deems, J.S., Schneider, D., Barsugli, J., Molotch, N., 2014. Filling in the gaps: inferring spatially distributed precipitation from gauge observations over complex terrain. Water Resour. Res. 50, http://dx.doi.org/10.1002/2014WR015442.

Lockwood, R., 2012. Where there's a Mill, There's a Way: Grand County Sawmills find Success in Beetle-kill Wood Markets. Colorado State Forest Service News. <http://csfs.colostate.edu/pdfs/FINAL-NR-SawmillsSuccessfulUsingBeetle-KillOct2012.pdf>.

Meddens, A.J., Hicke, J.A., Vierling, L.A., 2011. Evaluating the potential of multispectral imagery to map multiple stages of tree mortality. Remote Sens. Environ. 115 (7), 1632–1642.

Mesinger, F., DiMego, G., Kalnay, E., Mitchell, K., Shafran, P.C., Ebisuzaki, W., Jovic, D., Woollen, J., Rogers, E., Berbery, E.H., Ek, M.B., Fan, Y., Grumbine, R., Higgins, W., Li, H., Lin, Y., Manikin, G., Parrish, D., Shi, W., 2006. North American regional reanalysis. Bull. Am. Meteor. Soc. 87, 343–360. http://dx.doi.org/10.1175/BAMS-87-3-343.

Mikkelson, K.M., Maxwell, R.M., Ferguson, I., Stednick, J.D., McCray, J.E., Sharp, J.O., 2013. Mountain pine beetle infestation impacts: modeling water and energy budgets at the hill-slope scale. Ecohydrology 6, 64–72. http://dx.doi.org/10.1002/eco.278.

Molotch, N.P., 2009. Reconstructing snow water equivalent in the Rio Grande headwaters using remotely sensed snow cover data and a spatially distributed snowmelt model. Hydrol. Process. 23, 1076–1089. http://dx.doi.org/10.1002/hyp.7206.

Moriasi, D.N., Arnold, J.G., Van Liew, M.W., Bingner, R.L., Harmel, R.D., Veith, T.L., 2007. Model evaluation guidelines for systematic quantification of accuracy in watershed simulations. Trans. ASABE 50 (3), 885–900.

Nash, J.E., Sutcliffe, J.V., 1970. River flow forecasting through conceptual models Part I—A discussion of principles. J. Hydrol. 10 (3), 282–290.

Nijssen, B., Lettenmaier, D.P., 1999. A simplified approach for predicting shortwave radiation transfer through boreal forest canopies. J. Geophys. Res. Atmos. (1984–2012) 104 (D22), 27859–27868.

O'Halloran, T.L., Law, B.E., Goulden, M.L., Wang, Z., Barr, J.G., Schaaf, C., 2012. Radiative forcing of natural forest disturbances. Global Change Biol. doi: http://dx.doi.org/10.1111/j.1365-2486.2011.02577.x (in press).

Painter, T.H., Molotch, N.P., Cassidy, M., Flanner, M., Steffen, K., 2007. Contact spectroscopy for determination of stratigraphy of snow optical grain size. J. Glaciol. 53 (180), 121–127.

Painter, T.H., Deems, J.S., Belnap, J., Hamlet, A.F., Landry, C.C., Udall, B., 2010. Response of Colorado River runoff to dust radiative forcing in snow. Proc. Natl. Acad. Sci. 107 (40), 17125–17130. http://dx.doi.org/10.1073/pnas.0913139107.

Painter, T.H., Skiles, S.M., Deems, J.S., Bryant, A.C., Landry, C.C., 2012a. Dust radiative forcing in snow of the Upper Colorado River Basin: 1. A 6 year record of energy balance, radiation, and dust concentrations. Water Resour. Res. 48, W07521. http://dx.doi.org/10.1029/2012WR011985.

Painter, T.H., Bryant, A.C., Skiles, S.M., 2012b. Radiative forcing by light absorbing impurities in snow from MODIS surface reflectance data. Geophys. Res. Lett. 39 (17), L17502. http://dx.doi.org/10.1029/2012GL052457.

Pendall, E., Ewers, B., Norton, U., Brooks, P., Massman, W.J., Barnard, H., Frank, J., 2010. Impacts of beetle-induced forest mortality on carbon, water and nutrient cycling in the Rocky Mountains. FluxLetter 3, 17–21.

Perrot, D., Molotch, N.P., Musselman, K.N., Pugh, E.T., 2014. Modelling the effects of the mountain pine beetle on snowmelt in a subalpine forest. Ecohydrology 7, 226–241. http://dx.doi.org/10.1002/eco.1329.

Pielke Sr., R.A., Doesken, N., Bliss, O., Green, T., Chaffin, C., Salas, J.D., Woodhouse, C.A., Lukas, J.J., Wolter, K., 2005. Drought 2002 in Colorado: an unprecedented drought or a routine drought? Pure Appl. Geophys. 162, 1455–1479.

Potts, D.F., 1984. Hydrologic impacts of a large-scale mountain pine beetle (*Dendroctonus Ponderosae* Hopkins) epidemic. J. Am. Water Resour. Assoc. 20 (3), 373–377.

Pugh, E.T., Gordon, E.S., 2012. A conceptual model of water yield effects from beetle-induced tree death in snow-dominated lodgepole pine forests. Hydrol. Process. http://dx.doi.org/10.1002/hyp.9312.

Pugh, E.T., Small, E.E., 2012. The impact of pine beetle infestation on snow accumulation and melt in the headwaters of the Colorado River. Ecohydrology. http://dx.doi.org/10.1002/eco.239.

Pugh, E.T., Small, E.E., 2013. The impact of beetle-induced conifer death on stand-scale canopy snow interception. Hydrol. Res. 44 (4).

Ratzlaff, J.R., 1994. Mean annual precipitation, runoff, and runoff ratio for Kansas 1971–1990. Trans. Kansas Acad. Sci. (1903) 97 (3), 94–101.

Romme, W.H., Knight, D.H., Yavitt, J.B., 1986. Mountain pine beetle outbreaks in the Rocky Mountains: regulators of primary productivity? Am. Nat. 127 (4), 484–494.

Rudolph, J.A., 2012. Impacts of Beetle Kill on Modeled Streamflow Response in the North Platte River Basin Master's Thesis, University of Tennessee, 54 pp. <http://trace.tennessee.edu/utk_gradthes/1401>.

Schwarz, G.E., Alexander, R.B., 1995. State Soil Geographic (STATSGO) Database for the Conterminous United States, U.S. Geol. Surv. Open File Rep. 95-449, U.S. Geological Survey.

Simard, M., Romme, W.H., Griffin, J.M., Turner, M.G., 2011. Do mountain pine beetle outbreaks change the probability of active crown fire in lodgepole pine forests? Ecol. Monogr. 81 (1), 3–24.

Skiles, S.M., Painter, T.H., Deems, J.S., Bryant, A.C., Landry, C.C., 2012. Dust radiative forcing in snow of the Upper Colorado River Basin: 2. Interannual variability in radiative forcing and snowmelt rates,. Water Resour. Res. 48, W07522. http://dx.doi.org/10.1029/2012WR011986.

Somor, A.J., 2010. Quantifying Streamflow Change Following Bark Beetle Outbreak in Multiple Central Colorado Catchments. MS Thesis, Department of Hydrology and Water Resources, University of Arizona.

Stednick, J.D., Jensen, R., 2007. Effects of Pine Beetle Infestations on Water Yield and Water Quality at the Watershed Scale in Northern Colorado. Unpublished Technical Report. Report to CWRRI, Project 2007CO153B.

Stonesifer, C.S., 2007. Modeling the Cumulative Effects of Forest Fire on Watershed Hydrology: A Post-fire Application of the Distributed Hydrology Soil Vegetation Model (DHSVM). Master's Thesis, University of Montana.

Storck, P., Lettenmaier, D.P., Connelly, A., Cundy, T.W., 1995. Implication of Forest Practices on Downstream Flooding: Phase II Final Report. Washington Forest Protection Association, TFW-SH20-96-001.

Storck, P., Bowling, L., Weatherbee, P., Lettenmaier, D.P., 1998. Application of a GIS based distributed hydrology model for prediction of forest harvest effects on peak stream flow in the Pacific Northwest. Hydrol. Process. 12, 889–904.

Sun, G., Zhou, G., Zhang, Z., Wei, X., McNulty, S.G., Vose, J.M., 2006. Potential water yield reduction due to forestation across China. J. Hydrol. 328 (3), 548–558.

Thornton, P.E., Hasenauer, H., White, M.A., 2000. Simultaneous estimation of daily solar radiation and humidity from observed temperature and precipitation: an application over complex terrain in Austria. Agric. For. Meteorol. 104 (4), 255–271.

Thyer, M., Beckers, J., Spittlehouse, D., Alila, Y., Winkler, R., 2004. Diagnosing a distributed hydrologic model for two high-elevation forested catchments based on detailed stand-and basin-scale data. Water Resour. Res. 40 (1).

U.S. Army Corps of Engineers (USACE), 1956. Snow Hydrology: Summary Report of the Snow Investigations, U.S. Army of Engineers North Pacific Division, 437 pp.

Vlčková, M., Nechvátal, M., Soukup, M., 2009. Annual runoff coefficient in the Cerhovický stream catchment. J. Water Land. Dev. 13b, 41–56.

Vertessy, R.A., Hatton, T.J., O'Shaughnessy, P.J., Jayasuriya, M.D.A., 1993. Predicting water yield from a mountain ash forest catchment using a terrain analysis based catchment model. J. Hydrol. 150, 665–700.

Whitaker, A., Alila, Y., Beckers, J., Toews, D., 2003. Application of the distributed hydrology soil vegetation model to redfish creek, British Columbia: model evaluation using internal catchment data. Hydrol. Process. 17, 199–224.

White, J.C., Wulder, M.A., Brooks, D., Reich, R., Wheate, R.D., 2005. Detection of red attack stage mountain pine beetle infestation with high spatial resolution satellite imagery. Remote Sens. Environ. 96, 340–351.

Wigmosta, M.S., Vail, L.W., Lettenmaier, D.P., 1994. A distributed hydrology-vegetation model for complex terrain. Water Resour. Res. 30, 1665–1679.

Wigmosta, M.S., Perkins, W.A., 1998. A GIS-Based Modeling System for Watershed Analysis. Document Prepared for the National Council of the Paper Industry for Air and Stream Improvement Inc. (NCASI), Battelle Memorial Institute, Pacific Northwest Laboratories, Richland, WA.

Wulder, M.A., White, J.C., Bentz, B., Alvarez, M.F., Coops, N.C., 2006. Estimating the probability of mountain pine beetle red-attack damage. Remote Sens. Environ. 101, 150–166.

Zacharias, S., Wessolek, G., 2007. Excluding organic matter content from pedotransfer predictors of soil water retention. Soil Sci. Soc. Am. 71 (1), 43–50.